Supplementary Information

Wrinkled Ir-MnO_x nanospheres as pH-universal electrocatalysts for oxygen evolution reaction

Li Quan,[a] Yirong Cao,[a] Jinlong Liu,*[b] Bao Yu Xia, Xin Zhao,*[c] Bo You,*[a]

[a] Key Laboratory of Material Chemistry for Energy Conversion and Storage Ministry of Education, Hubei Key Laboratory of Material Chemistry and Service Failure, School of Chemistry and Chemical Engineering, Huazhong University of Science and Technology, Wuhan, Hubei 430074, China. Email: youbo@hust.edu.cn

[b] College of Chemistry and Chemical Engineering, Central South University, Changsha, Hunan 410083, China. E-mail: liujinlong@csu.edu.cn

[c] Hubei Engineering Research Center of Radio Frequency Microwave Technology and Application, School of Science, Wuhan University of Technology, Wuhan, Hubei 430070, China. Email: xzhao@whut.edu.cn

Methods

Chemicals: Perchloric acid ($HClO_4$, 70%) and Nafion (5 wt%, 50 μL) were purchased from Sigma-Aldrich. Commercial iridium(iv) oxide (IrO_2), sodium iridium chloride ($Na_3IrCl_6 \cdot xH_2O$), manganese nitrate ($Mn(NO_3)_2 \cdot 4H_2O$), and ethanol were purchased from Shanghai Aladdin Bio-Chem Technology Co., Ltd. Trimesic acid ($C_6H_3(COOH)_3$), lauric acid, and methanol were purchased from Shanghai Macklin Biochemical Co., Ltd.

Preparation of Ir-doped Mn-MIL-100: Ir-doped Mn-MIL-100 was prepared by solvothermal method. 0.12 mmol $Mn(NO_3)_2 \cdot 4H_2O$, 0.02 mmol $Na_3IrCl_6 \cdot xH_2O$ and 0.475 mmol $C_6H_3(COOH)_3$, 2.25 mmol lauric acid were dissolved in 25 mL methanol, and stirred at 800 rpm for 10 min. The mixture was then transferred to a 50 mL stainless-steel autoclave and heated to 125 °C for 2 h. After cooling to room temperature, the mixture was centrifuged, washed and dried under vacuum at 60 °C. For comparison, Mn-MIL-100 was also synthesized by the same method, without the addition of $Na_3IrCl_6 \cdot xH_2O$.

Preparation of Ir-MnO$_x$ and control sample: Ir-MnO$_x$ was obtained by annealing Ir-doped Mn-MIL-100 at 450 °C for 3 h in a muffle furnace. Similarly, Mn_2O_3 was obtained by annealing Mn-MIL-100 in a muffle furnace at the same temperature.

Characterizations: The morphology and chemical composition of the as-prepared samples were characterized by scanning electron microscope (SEM, TESCAN VEGA 3 SBH), transmission electron microscopy (TEM, Tecnai G2 F30), and energy dispersive spectrum (EDS mapping). X-ray photoelectron spectroscopy (XPS) was performed on an AXIS-ULTRA DLD-600W X-ray photoelectron spectrometer using Mg as the exciting source. The Ir content in electrocatalysts was measured by inductively coupled plasma-atomic emission spectrometry on an iCAP-7200plus system. The characteristic diffraction peaks of the products were identified by X-ray diffraction (XRD, Rigaku SmartLab-SE).

Electrochemical measurements: All electrochemical performance tests were carried out on an electrochemical workstation (CHI 760E, CH Instrument) using a three-electrode configuration with graphite rod as the counter electrode, Ag/AgCl (saturated KCl electrolyte) electrode as the reference electrode and RRDE (Pine Research Instrumentation, collection efficiency is 0.37) as the working electrode. The catalysts-loaded working electrode was prepared as follows: 1 mg catalyst and 1 mg carbon black (XC 72) were dispersed in 1 mL mixed solution containing 580 μL ethanol, 400 μL deionized water and 20 μL Nafion. After uniform dispersion by ultrasonication for 30 min, 25 μL homogeneous catalysts ink was deposited on the electrode and air-dried for subsequent electrochemical testing. The polarization curve of OER was obtained in O_2-saturated electrolytes at a scan rate of 5 mV s^{-1}, and the stability of the electrocatalysts was assessed by chronopotentiometric measurements. All corresponding potentials were calibrated to the reversible standard hydrogen electrode (RHE).

Electrocatalytic activity can be described in terms of mass activity and turnover frequency (TOF). The mass activity can be calculated according to the following equation:

$$Mass\ activity = \frac{i}{m_{Ir}}$$

where i is the current during OER measurement at an applied potential, and m_{Ir} is the mass of Ir loaded on the electrode.

The TOF can be calculated according to the following equation:

$$TOF = \frac{i}{4 * F * n}$$

where 4 is the number of electrons transferred in a OER process, n is the moles number of active sites, and F is the Faraday constant. The n of an electrocatalyst was determined by the following equation:

$$n = \frac{m_{Ir}}{M_{Ir}}$$

Where M_{Ir} is the molar mass of Ir.

***Operando* ATR-SEIRS measurements:** *Operando* attenuated total reflection surface-enhanced Fourier-transform infrared spectroscopy (ATR-SEIRS) measurements were performed on Nicolet iS50R FTIR Spectrometer to identify the potential-dependent intermediates and reaction mechanism. This was carried out using a three-electrode system in an H-cell with 1 M $HClO_4$ as the electrolyte, Ag/AgCl as the reference electrode, a Pt foil as the counter electrode, and a catalyst loaded Au-coated Si ATR wafer as the working electrode. The background was subtracted at the open circuit potential and the spectra were collected between 1000 and 4000 cm^{-1} at different potentials.

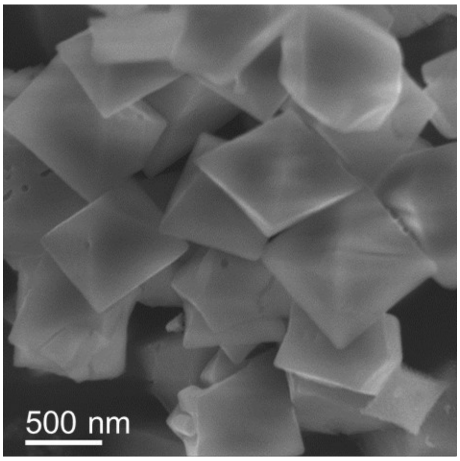

Fig. S1 SEM image of Mn-MIL-100.

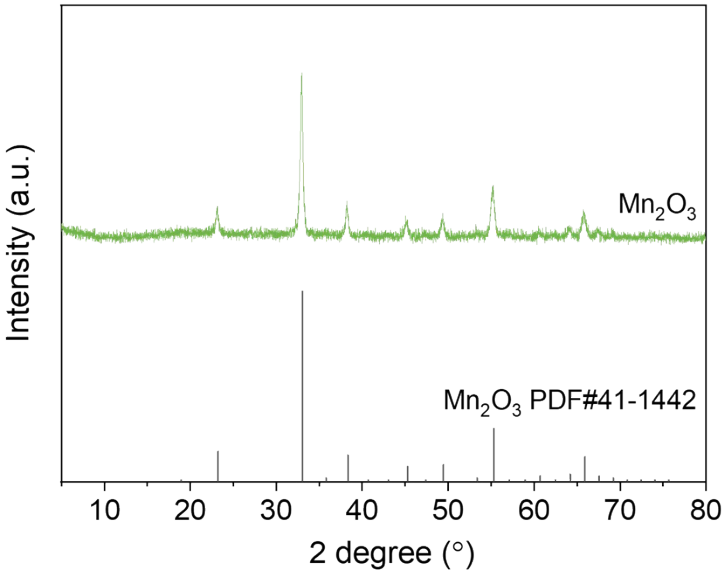

Fig. S2 XRD pattern of Mn-MIL-100-derived Mn_2O_3.

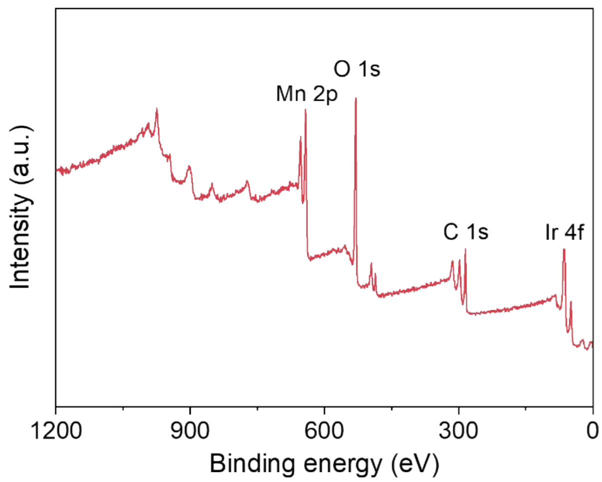

Fig. S3 XPS survey spectrum of Ir-MnO_x.

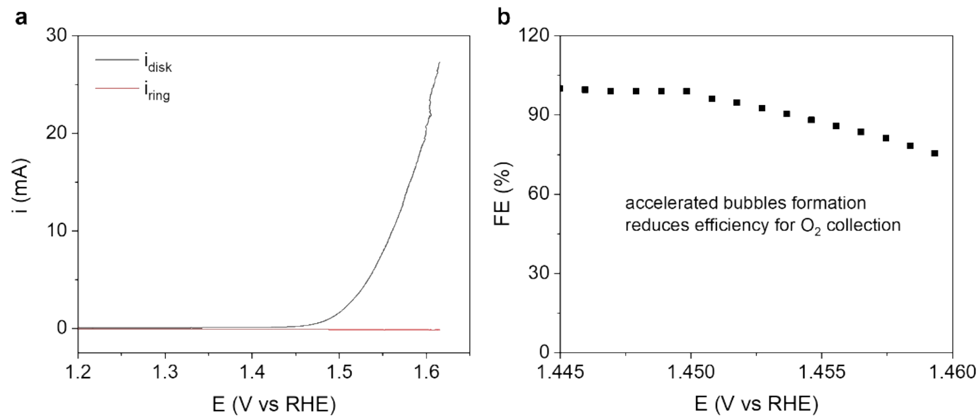

Fig. S4 Determination of the Faradaic efficiency of OER for Ir-MnO_x. (a) Disk and ring currents, and (b) Faradaic efficiency of O_2 for Ir-MnO_x. *Linear potential scanning was conducted at the disk electrode, while the ring was held at 0.1 V vs. RHE. The rotation speed of RRDE was set at 1600 rpm. The decreased O_2 collection efficiency is attributed to the massive O_2 bubble formation at the disk electrode when increasing the applied potential which cannot be collected by the ring electrode completely*.

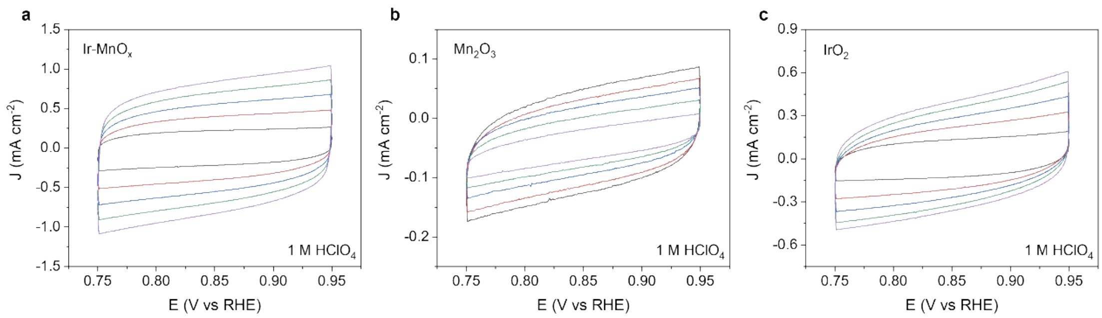

Fig. S5 Cyclic voltammograms of (a) Ir-MnO$_x$, (b) Mn_2O_3, and (c) IrO_2 at scan rates from 20 to 100 mV s^{-1} in a non-Faradaic potential region in 1 M $HClO_4$ electrolyte for estimating the ECSA.

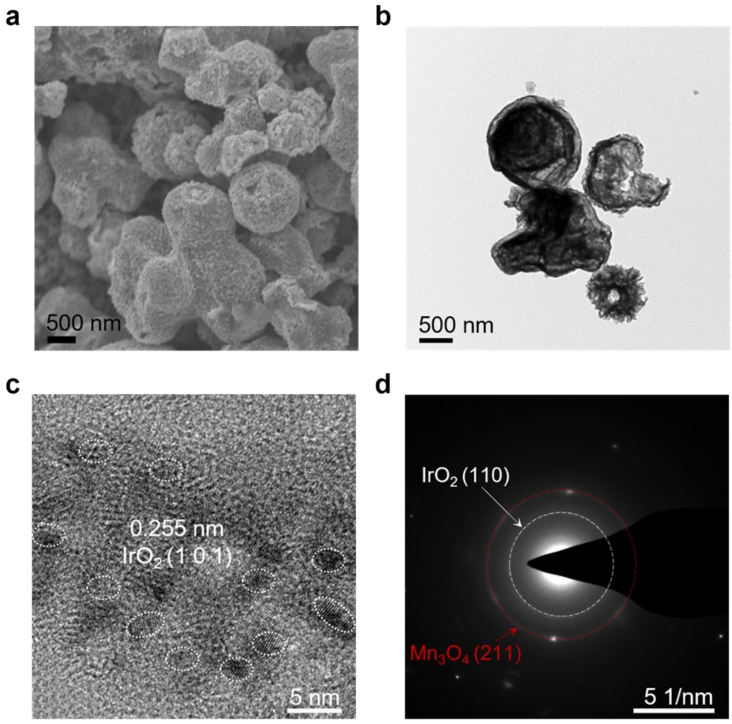

Fig. S6 (a) SEM image, (b) TEM image, (c) HRTEM image and (d) SAED pattern of post-OER Ir-MnO_x.

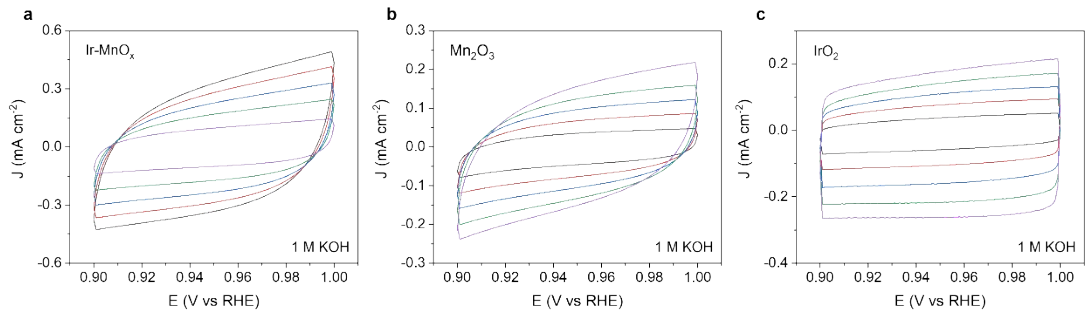

Fig. S7 Cyclic voltammograms of (a) Ir-MnO_x, (b) Mn_2O_3, and (c) IrO_2 at scan rates from 20 to 100 mV s^{-1} in a non-Faradaic potential region in 1 M KOH electrolyte for estimating the ECSA.

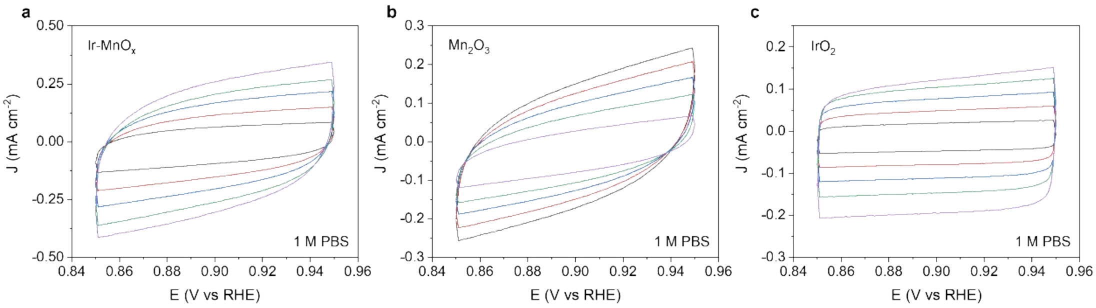

Fig. S8 Cyclic voltammograms of (a) Ir-MnO_x, (b) Mn_2O_3, and (c) IrO_2 at scan rates from 20 to 100 mV s^{-1} in a non-Faradaic potential region in 1 M PBS electrolyte for estimating the ECSA.

Table S1. Summary of the performance of OER electrocatalysts in acidic media.

OER electrocatalyst	***η* (10 mA cm^{-2})**	**Stability (h)**	**Ref.**
Ir-MnO_x	270 mV	40	This work
Ir nanotube	245 mV	4	S1
3D Ir superstructure	270 mV	8	S2
Ir wavy nanowires	270 mV	7	S3
Ir nanosheets	240 mV	8	S4
Co–RuIr nanocrystals	235 mV	25	S5
$Ir_{44}Pd_{10}$ nanocage	226 mV	15	S6
P–$IrCu_{1.4}$	311 mV	10	S7
$Ir_{0.6}Cr_{0.4}O_x$ nanowires	250 mV	25	S8
IrOOH nanosheets	344 mV	14	S9
$Ni_{0.34}Co_{0.46}Ir_{0.2}O_{\varphi}$	280 mV	5.6	S10
Ir-CCTO	280 mV	20	S11
Ir-HTO	266 mV	50	S12
$Pr_2Ir_2O_7$	290 mV	3	S13
Mn–RuIr NCT	198 mV	10	S14
sl-$Mn_{0.98}Ir_{0.02}O_2$	105 mV	>48	S15
Ir–MnO_2	218 mV	650	S16
12Ru/MnO_2	161 mV	200	S17
$Mn_{0.73}Ru_{0.27}O_{2-\delta}$	208 mV	10	S18
Ir-$NiCo_2O_4$	240 mV	70	S19
IrRuMn/C	260 mV	8	S20
$Ir_{0.06}Co_{2.94}O_4$	292 mV	200	S21
$SrCo_{0.9}Ir_{0.1}O_3$	290 mV	3	S22
IrO_2 NN-L	313 mV	2	S23

Table S2. Summary of the performance of OER electrocatalysts in alkaline media.

OER electrocatalyst	***η* (10 mA cm^{-2})**	**Stability (h)**	**Ref.**
Ir-MnO_x	295 mV	80	This work
Co-Mn LDH	325 mV	14	S24
$MnCo_2O_4$@Ni_2P	240 mV	20	S25
Mn@CoMnO	246 mV	40	S26
$Mn_xCo_{3-x}O_4$	327 mV	25	S27
$CoMn_2O_4$	310 mV	24	S28
Mn_2Co_2C/MnO	320 mV	10	S29
Mn-NSG	296 mV	70	S30
Mn-NG	337 mV	120	S31
$CDs_{0.15}$-MnO_2	343 mV	36	S32
Ni–Mn_3O_4	283 mV	1	S33
HEO (CoFeNiCrMn)	307 mV	168	S34
$Sr_2Fe_{0.8}Co_{0.2}Mo_{0.6}Co_{0.4}O_{6-\delta}$	345 mV	15	S35
$MnFeCoNiO_x$	302 mV	20	S36
$(Co,Cu,Fe,Mn,Ni)_3O_4$	350 mV	12	S37
$K_{0.8}Na_{0.2}(MgMnFeCoNi)F_3$	314 mV	10	S38
$(Co_{0.2}Mn_{0.2}Ni_{0.2}Fe_{0.2}Zn_{0.2})Fe_2O_4$	326 mV	10	S39
$(CoNiMnZnFe)_3O_{3.2}$	336 mV	20	S40
$La(CrMnFeCo_2Ni)O_3$	325 mV	50	S41

Table S3. Summary of the performance of OER electrocatalysts in neutral media.

OER electrocatalyst	***η*** **(10 mA cm^{-2})**	**Stability (h)**	**Ref.**
Ir-MnO_x	360 mV	24	This work
Ir-NSG	307 mV	4.2	S42
Ir(0.3)CoFe LDH	323 mV	24	S43
$Ir_{0.43}Mo_{0.57}O_2$	266 mV	12	S44
P-IrO_x@DG	340 mV	N.A.	S45
$Ir_{0.48}Cu_{0.52}O_y$	328 mV	5.5	S46
BPIr-be	620 mV	N.A.	S47
$Ni_{0.1}Co_{0.9}$P-CFP	550 mV	20	S48
RhCo	310 mV	5	S49
Ir_1-$Co(OH)_2$	373 mV	10	S50
Co-Pi/Ti	450 mV	20	S51
S-$NiFe_2O_4$/NF	494 mV	N.A.	S52
CoP NA/CC	536 mV	35	S53
$Ni(S_{0.5}Se_{0.5})_2$	501 mV	20	S54
Co_4Mo	490 mV	15	S55

Supplementary References

S1. J.-Y. Zhu, Q. Xue, Y.-Y. Xue, Y. Ding, F.-M. Li, P. Jin, P. Chen and Y. Chen, *ACS Appl. Mater. Interfaces*, 2020, **12**, 14064-14070.

S2. Y. Pi, N. Zhang, S. Guo, J. Guo and X. Huang, *Nano Lett.*, 2016, **16**, 4424-4430.

S3. L. Fu, F. Yang, G. Cheng and W. Luo, *Nanoscale*, 2018, **10**, 1892-1897.

S4. B. Jiang, Y. Guo, J. Kim, A. E. Whitten, K. Wood, K. Kani, A. E. Rowan, J. Henzie and Y. Yamauchi, *J. Am. Chem. Soc.*, 2018, **140**, 12434-12441.

S5. J. Shan, T. Ling, K. Davey, Y. Zheng and S.-Z. Qiao, *Adv. Mater.*, 2019, **31**, 1900510.

S6. J. Zhu, Z. Chen, M. Xie, Z. Lyu, M. Chi, M. Mavrikakis, W. Jin and Y. Xia, *Angew. Chem. Int. Ed.*, 2019, **58**, 7244-7248.

S7. Y. Pi, J. Guo, Q. Shao and X. Huang, *Chem. Mater.*, 2018, **30**, 8571-8578.

S8. W. Gou, M. Zhang, Y. Zou, X. Zhou and Y. Qu, *ChemCatChem*, 2019, **11**, 6008-6014.

S9. D. Weber, L. M. Schoop, D. Wurmbrand, S. Laha, F. Podjaski, V. Duppel, K. Müller, U. Starke and B. V. Lotsch, *J. Mater. Chem. A*, 2018, **6**, 21558-21566.

S10. W. Q. Zaman, W. Sun, M. Tariq, Z. Zhou, U. Farooq, Z. Abbas, L. Cao and J. Yang, *Appl. Catal. B: Environ.*, 2019, **244**, 295-302.

S11. N. T. T. Thao, K. Kim, J. H. Ryu, B.-S. An, A. K. Nayak, J. U. Jang, K.-H. Na, W.-Y. Choi, G. Ali, K. H. Chae, M. Akbar, K. Y. Chung, H.-S. Cho, J. H. Park, B.-H. Kim and H. Han, *Adv. Sci.*, 2023, **10**, 2207695.

S12. S. Y. Jung, K. M. Kim, J. H. Ryu, S. Yeo, H. Jeon, A. K. Nayak, N. Thi Thu Thao, E. Enkhtuvshin, S. J. Kim, J. U. Jang, M. G. Kim, K.-H. Na, W.-Y. Choi, J. Bang, S. Choi, T. Song, S. Mhin and H. Han, *J. Alloys Compd.*, 2023, **946**, 169466.

S13. C. Shang, C. Cao, D. Yu, Y. Yan, Y. Lin, H. Li, T. Zheng, X. Yan, W. Yu, S. Zhou and J. Zeng, *Adv. Mater.*, 2019, **31**, 1805104.

S14. J. Joo, Y. Park, J. Kim, T. Kwon, M. Jun, D. Ahn, H. Baik, J. H. Jang, J. Y. Kim and K. Lee, *Small Methods*, 2022, **6**, 2101236.

S15. W. Zhao, F. Xu, L. Liu, M. Liu and B. Weng, *Adv. Mater.*, 2023, **35**, 2308060.

S16. Z. Shi, Y. Wang, J. Li, X. Wang, Y. Wang, Y. Li, W. Xu, Z. Jiang, C. Liu, W. Xing and J. Ge, *Joule*, 2021, **5**, 2164-2176.

S17. C. Lin, J.-L. Li, X. Li, S. Yang, W. Luo, Y. Zhang, S.-H. Kim, D.-H. Kim, S. S. Shinde, Y.-F. Li, Z.-P. Liu, Z. Jiang and J.-H. Lee, *Nat. Catal.*, 2021, **4**, 1012-1023.

S18. K. Wang, Y. Wang, B. Yang, Z. Li, X. Qin, Q. Zhang, L. Lei, M. Qiu, G. Wu and Y. Hou, *Energy Environ. Sci.*, 2022, **15**, 2356-2365.

S19. J. Yin, J. Jin, M. Lu, B. Huang, H. Zhang, Y. Peng, P. Xi and C.-H. Yan, *J. Am. Chem. Soc.*, 2020, **142**, 18378-18386.

S20. M. Aizaz Ud Din, S. Irfan, S. U. Dar and S. Rizwan, *Chem. Eur. J.*, 2020, **26**, 5662-5666.

S21. J. Shan, C. Ye, S. Chen, T. Sun, Y. Jiao, L. Liu, C. Zhu, L. Song, Y. Han, M. Jaroniec, Y. Zhu, Y. Zheng and S.-Z. Qiao, *J. Am. Chem. Soc.*, 2021, **143**, 5201-5211.

S22. Y. Chen, H. Li, J. Wang, Y. Du, S. Xi, Y. Sun, M. Sherburne, J. W. Ager, A. C. Fisher and Z. J. Xu, *Nat. Commun.*, 2019, **10**, 572.

S23. J. Lim, D. Park, S. S. Jeon, C.-W. Roh, J. Choi, D. Yoon, M. Park, H. Jung and H. Lee, *Adv. Funct. Mater.*, 2018, **28**, 1704796.

S24. F. Song and X. Hu, *J. Am. Chem. Soc.*, 2014, **136**, 16481-16484.

S25. J. Ge, W. Zhang, J. Tu, T. Xia, S. Chen and G. Xie, *Small*, 2020, **16**, 2001856.

S26. C. Hu, L. Zhang, Z.-J. Zhao, J. Luo, J. Shi, Z. Huang and J. Gong, *Adv. Mater.*, 2017, **29**, 1701820.

S27. K. Lankauf, K. Cysewska, J. Karczewski, A. Mielewczyk-Gryń, K. Górnicka, G. Cempura, M. Chen, P. Jasiński and S. Molin, *Int. J. Hydrogen Energy*, 2020, **45**, 14867-14879.

S28. A. Bahadur, W. Hussain, S. Iqbal, F. Ullah, M. Shoaib, G. Liu and K. Feng, *J. Mater. Chem. A*, 2021, **9**, 12255-12264.

S29. T. Meng and M. Cao, *ACS Sustain. Chem. Eng.*, 2020, **8**, 13271-13281.

S30. X. Bai, L. Wang, B. Nan, T. Tang, X. Niu and J. Guan, *Nano Res.*, 2022, **15**, 6019-6025.

S31. J. Guan, Z. Duan, F. Zhang, S. D. Kelly, R. Si, M. Dupuis, Q. Huang, J. Q. Chen, C. Tang and C. Li, *Nat. Catal.*, 2018, **1**, 870-877.

S32. L. Tian, J. Wang, K. Wang, H. Wo, X. Wang, W. Zhuang, T. Li and X. Du, *Carbon*, 2019, **143**, 457-466.

S33. V. Maruthapandian, T. Pandiarajan, V. Saraswathy and S. Muralidharan, *RSC Adv.*, 2016, **6**, 48995-49002.

S34. J. Baek, M. D. Hossain, P. Mukherjee, J. Lee, K. T. Winther, J. Leem, Y. Jiang, W. C. Chueh, M. Bajdich and X. Zheng, *Nat. Commun.*, 2023, **14**, 5936.

S35. H. Sun, X. Xu, G. Chen, Y. Zhou, H.-J. Lin, C.-T. Chen, R. Ran, W. Zhou and Z. Shao, *ChemSusChem*, 2019, **12**, 5111-5116.

S36. W. Dai, T. Lu and Y. Pan, *J. Power Sources*, 2019, **430**, 104-111.

S37. D. Wang, Z. Liu, S. Du, Y. Zhang, H. Li, Z. Xiao, W. Chen, R. Chen, Y. Wang, Y. Zou and S. Wang, *J. Mater. Chem. A*, 2019, **7**, 24211-24216.

S38. T. Wang, H. Chen, Z. Yang, J. Liang and S. Dai, *J. Am. Chem. Soc.*, 2020, **142**, 4550-4554.

S39. Y. Zhang, T. Lu, Y. Ye, W. Dai, Y. a. Zhu and Y. Pan, *ACS Appl. Mater. Interfaces*, 2020, **12**, 32548-32555.

S40. Y. Zhang, W. Dai, P. Zhang, T. Lu and Y. Pan, *J. Alloys Compd.*, 2021, **868**, 159064.

S41. T. X. Nguyen, Y.-C. Liao, C.-C. Lin, Y.-H. Su and J.-M. Ting, *Adv. Funct. Mater.*, 2021, **31**, 2101632.

S42. Q. Wang, C.-Q. Xu, W. Liu, S.-F. Hung, H. Bin Yang, J. Gao, W. Cai, H. M. Chen, J. Li and B. Liu, *Nat. Commun.*, 2020, **11**, 4246.

S43. J. M. Yu, J. Song, Y. K. Kim, J. Oh, K. Y. Kim, W. Y. Noh, W. J. Byun, J. U. Lee, C. Yang, J.-W. Jang, J. S. Lee and S. Cho, *Nano Lett.*, 2023, **23**, 5092-5100.

S44. S. H. Ahn, D. Jin, C. Lee and Y. Lee, *J. Mater. Chem. A*, 2023, **11**, 14941-14951.

S45. L. Zhuang, F. Xu, K. Wang, J. Li, C. Liang, W. Zhou, Z. Xu, Z. Shao and Z. Zhu, *Small*, 2021, **17**, 2100121.

S46. Y. Kim, D. Jin, C. Lee and Y. Lee, *J. Alloys Compd.*, 2022, **909**, 164813.

S47. J. Mei, T. He, J. Bai, D. Qi, A. Du, T. Liao, G. A. Ayoko, Y. Yamauchi, L. Sun and Z. Sun, *Adv. Mater.*, 2021, **33**, 2104638.

S48. R. Wu, B. Xiao, Q. Gao, Y.-R. Zheng, X.-S. Zheng, J.-F. Zhu, M.-R. Gao and S.-H. Yu, *Angew. Chem. Int. Ed.*, 2018, **57**, 15445-15449.

S49. Y. Zhao, J. Bai, X.-R. Wu, P. Chen, P.-J. Jin, H.-C. Yao and Y. Chen, *J. Mater. Chem. A*, 2019, **7**, 16437-16446.

S50. Y. Zhang, C. Wu, H. Jiang, Y. Lin, H. Liu, Q. He, S. Chen, T. Duan and L. Song, *Adv. Mater.*, 2018, **30**, 1707522.

S51. L. Xie, R. Zhang, L. Cui, D. Liu, S. Hao, Y. Ma, G. Du, A. M. Asiri and X. Sun, *Angew. Chem. Int. Ed.*, 2017, **56**, 1064-1068.
S52. J. Liu, D. Zhu, T. Ling, A. Vasileff and S.-Z. Qiao, *Nano Energy*, 2017, **40**, 264-273.
S53. T. Liu, L. Xie, J. Yang, R. Kong, G. Du, A. M. Asiri, X. Sun and L. Chen, *ChemElectroChem*, 2017, **4**, 1840-1845.
S54. L. Zeng, K. Sun, Y. Chen, Z. Liu, Y. Chen, Y. Pan, R. Zhao, Y. Liu and C. Liu, *J. Mater. Chem. A*, 2019, **7**, 16793-16802.
S55. Y.-T. Xu, Z.-M. Ye, J.-W. Ye, L.-M. Cao, R.-K. Huang, J.-X. Wu, D.-D. Zhou, X.-F. Zhang, C.-T. He, J.-P. Zhang and X.-M. Chen, *Angew. Chem. Int. Ed.*, 2019, **58**, 139-143.